Communication

Deciphering the Disaggregation Mechanism of Amyloid Beta Aggregate by 4-(2-Hydroxyethyl)-1-Piperazinepropanesulfonic Acid Using Electrochemical Impedance Spectroscopy

Hien T. Ngoc Le [1] and Sungbo Cho [1,2,*]

1   Department of Electronic Engineering, Gachon University, Seongnam-si, Gyeonggi-do 13120, Korea; ltnh1809@gachon.ac.kr
2   Department of Health Sciences and Technology, GAIHST, Gachon University, Incheon 21999, Korea
*   Correspondence: sbcho@gachon.ac.kr; Tel.: +82-(31)-750-5321

Abstract: Aggregation of amyloid-β (aβ) peptides into toxic oligomers, fibrils, and plaques is central in the molecular pathogenesis of Alzheimer's disease (AD) and is the primary focus of AD diagnostics. Disaggregation or elimination of toxic aβ aggregates in patients is important for delaying the progression of neurodegenerative disorders in AD. Recently, 4-(2-hydroxyethyl)-1-piperazinepropanesulfonic acid (EPPS) was introduced as a chemical agent that binds with toxic aβ aggregates and transforms them into monomers to reduce the negative effects of aβ aggregates in the brain. However, the mechanism of aβ disaggregation by EPPS has not yet been completely clarified. In this study, an electrochemical impedimetric immunosensor for aβ diagnostics was developed by immobilizing a specific anti-amyloid-β (aβ) antibody onto a self-assembled monolayer functionalized with a new interdigitated chain-shaped electrode (anti-aβ/SAM/ICE). To investigate the ability of EPPS in recognizing AD by extricating aβ aggregation, commercially available aβ aggregates ($a\beta_{agg}$) were used. Electrochemical impedance spectroscopy was used to probe the changes in charge transfer resistance (R_{ct}) of the immunosensor after the specific binding of biosensor with $a\beta_{agg}$. The subsequent incubation of the $a\beta_{agg}$ complex with a specific concentration of EPPS at different time intervals divulged AD progression. The decline in the R_{ct} of the immunosensor started at 10 min of EPPS incubation and continued to decrease gradually from 20 min, indicating that the accumulation of $a\beta_{agg}$ on the surface of the anti-aβ/SAM/ICE sensor has been extricated. Here, the kinetic disaggregation rate k value of $a\beta_{agg}$ was found to be 0.038. This innovative study using electrochemical measurement to investigate the mechanism of $a\beta_{agg}$ disaggregation by EPPS could provide a new perspective in monitoring the disaggregation periods of $a\beta_{agg}$ from oligomeric to monomeric form, and then support for the prediction and handling AD symptoms at different stages after treatment by a drug, EPPS.

Keywords: Alzheimer's disease; amyloid beta aggregate; 4-(2-hydroxyethyl)-1-piperazinepropanesulfonic acid; impedimetric immunosensor; electrochemical impedance spectroscopy; kinetic disaggregation of protein

1. Introduction

The deposition of the amyloid-β (aβ) protein in the cortex of the brain is reported as a leading cause of Alzheimer's disease (AD), the most common form of dementia [1]. According to the amyloid cascade hypothesis, aβ peptides tend to aggregate and coalesce into toxic insoluble oligomers and fibrils in plaques, which may cause decline in synaptic function and nerve cell damage [2,3].

Aggregation of aβ gradually increases throughout the brain, which leads to neurodegeneration, starting from mild to moderate symptoms in earlier Alzheimer's stages, and finally dementia [3,4]. Many efforts have been made to control and prevent Alzheimer's progression by inhibiting and reducing the aggregation of aβ. For instance, laser-induced

destruction [5], ultrasonic treatment [6], temperature-induced dissociation [7], pulsed radio-frequency cold atmospheric plasma jet [8], and drug treatments [9,10] have all been used to eliminate the aggregation of aβ. Among these approaches, drug treatment is the most-studied means of reducing or eliminating aβ aggregation, as these agents provide the most practical strategy to target the aβ aggregates within the body. Some natural chemical compounds such as theaflavins from black tea, epigallocatechin 3-gallate from green tea, and components from coffee showed an inhibitory effect on the aggregation of aβ [11–13]. However, the precise mechanism of interaction between these agents and aβ aggregates remains uncertain, and none of these have been used to treat AD clinically.

Recently, 4-(2-hydroxyethyl)-1-piperazinepropanesulfonic acid (EPPS) has been acknowledged as a promising drug candidate for dissociating and converting aβ aggregates into monomers. A study on a mouse model of Alzheimer's aβ plaques found that EPPS can contribute to the breakdown of the plaques, which can alleviate some of the AD symptoms in mice [14]. Despite its significance, the detailed mechanism of EPPS on the disaggregation of aβ aggregates has not been thoroughly elucidated.

Electrochemical immunosensors offer rapid response, high sensitivity, and selective detection of aβ at very low concentrations [15–18]. In this report, we created an impedimetric immunosensor for the diagnosis of aβ aggregates ($a\beta_{agg}$) and aβ peptide ($a\beta_{pep}$). It was produce by the immobilization of a specific anti-aβ antibody on a self-assembled monolayer functionalized with a new interdigitated chain-shaped electrode (anti-aβ/SAM/ICE). This was then used to monitor the effect of EPPS on the disaggregation $a\beta_{agg}$. After the anti-aβ/SAM/ICE biosensor bound with $a\beta_{agg}$, forming the $a\beta_{agg}$ complex, the $a\beta_{agg}$ complex was then incubated with a specific concentration of EPPS at different time intervals to divulge the disaggregation progress of $a\beta_{agg}$. Electrochemical impedance spectroscopy (EIS) was used as a tool to confirm the changes in charge transfer resistance (R_{ct}) of the immunosensor after forming the complex and EPPS treatment. We established a new method for studying the mechanism of EPPS-induced kinetic disaggregation of $a\beta_{agg}$ by analyzing the EIS results from this study, leading to new insights in the diagnostics and treatment of AD symptoms at various levels.

2. Materials and Methods

2.1. Materials

AggreSure^{TM} Amyloid-β 1–42 aggregate ($a\beta_{agg}$) is bought from AnaSpec (Fremont, CA 94555, USA). Anti-aβ antibody ab126649 (anti-aβ), Amyloid beta peptide 1–42, human, ab120301 ($a\beta_{pep}$) are bought from Abcam (Seoul, Korea).

De-ionized (DI) water is gained from Milli-Q system. Phosphate buffer saline (PBS, pH 7.4) is received from Tech-Innovation.

4-(2-hydroxyethyl)-1-piperazinepropanesulfonic acid (EPPS, BioXtra, ≥99.5% [titration]), EDC hydrochloride (crystalline, ≥98.0%), 6-mercaptohexanoic acid (MHA, 90%), 1-hydroxy-2,5-pyrrolidinedione (NHS, 98.0%), potassium ferrocyanide/ferricyanide ($[Fe(CN)_6]^{3-/4-}$), bovine serum albumin (BSA, 0.5% in 1 × PBS, pH 7.4) are obtained from Sigma Aldrich (Seoul, Korea).

2.2. Development of the Immunosensor for Monitoring the Impact of EPPS on the Disaggregation of $a\beta_{agg}$

On a glass transparency substrate (13.5 × 16.0 mm), an interdigitated chain-shaped electrode (ICE) is made. Ti and Au have been deposited in an electron beam-evaporator with electrodes 25 nm and 50 nm of thickness. The lift-off procedure then formed the coupled electrode finger consisting of 5 μm distance and width for working and reference electrodes. The ICE was then cleaned with 100% ethanol, DI water, and dried in nitrogen gas flow to prepare for the development of the immunosensor. Schematic of the fabrication and microscope image of ICE are displayed in Figure 1.
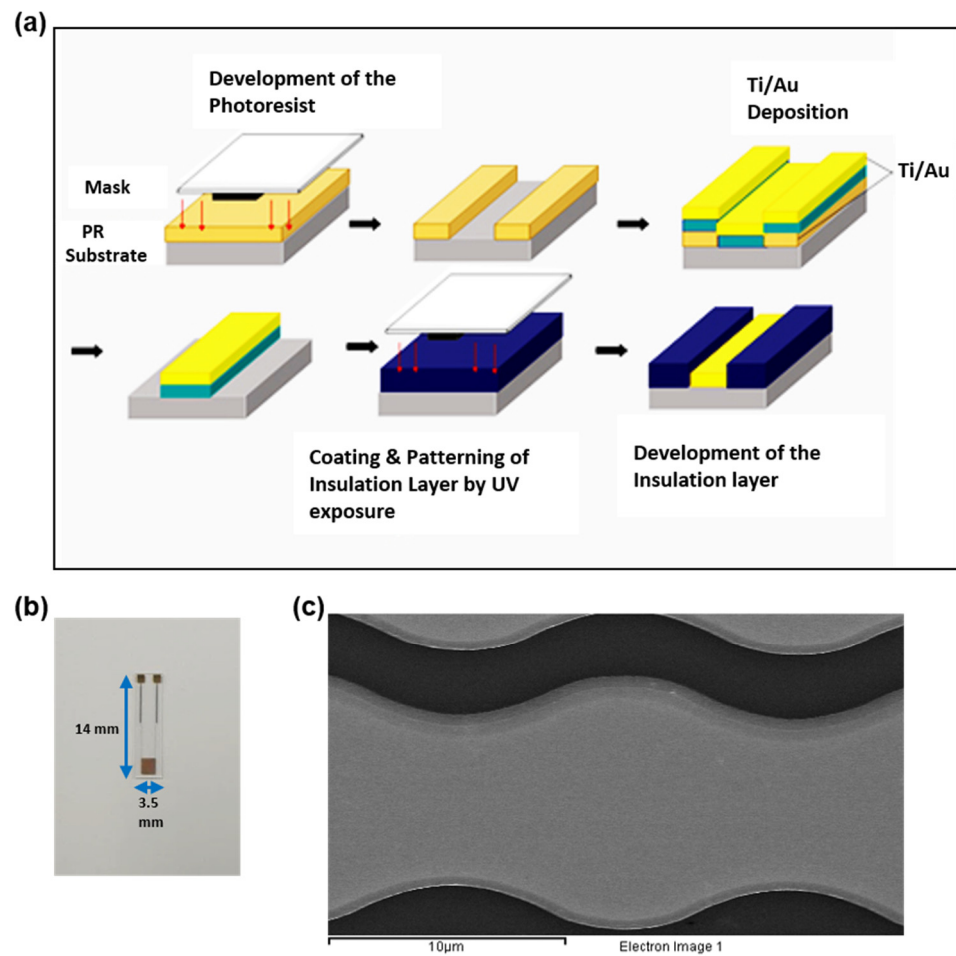
Figure 1. (**a**) Fabrication of ICE, (**b**) Photograph of ICE, and (**c**) Scanning electron microscope image of chain-shaped gold finger of ICE.

The development of the immunosensor for diagnosis of $a\beta_{agg}$ is displayed in Figure 2. A self-assembled monolayer (SAM) has been mounted on the purified ICE gold surface in 100 mM MHA for 24 hours at room temperature. A solution of 75 mM EDC and 5 mM NHS was then incubated with the SAM-modified electrode to activate the carboxyl group for antibody binding. Then, ten anti-$a\beta$ antibody microliters (100 $\mu g \cdot mL^{-1}$) in PBS (pH ~ 7.4) are dripped off into a modified electrode and incubated for 1 hour in a moist compartment at 4 °C. Therefore, the EDC/NHS-activated SAM molecules on the modified electrodes were attached to the anti-$a\beta$ antibody through the amino group. After that, nonspecific adsorption was blocked by incubating with BSA (0.5% in 1 × PBS, pH 7.4) for 20 min at 4 °C to develop the anti-$a\beta$/SAM/ICE biosensor. The developed anti-$a\beta$/SAM/ICE biosensor was then incubated with $a\beta_{agg}$ (in PBS (pH ~ 7.4)) for 20 min at room temperature for the recognition of $a\beta_{agg}$.

To monitor the effect of EPPS on the kinetics disaggregation of $a\beta_{agg}$, the anti-$a\beta$/SAM/ICE biosensor was incubated with $a\beta_{agg}$ (2.5×10^{-3} $mg \cdot mL^{-1}$) for 20 min to enable a specific binding between the antibody and antigen, called the $a\beta_{agg}$ complex. Subsequently, the $a\beta_{agg}$ complex was incubated with 20 $mM \cdot L^{-1}$ of EPPS for various time periods to study the disaggregation process of $a\beta_{agg}$ by electrochemical impedance measurement.
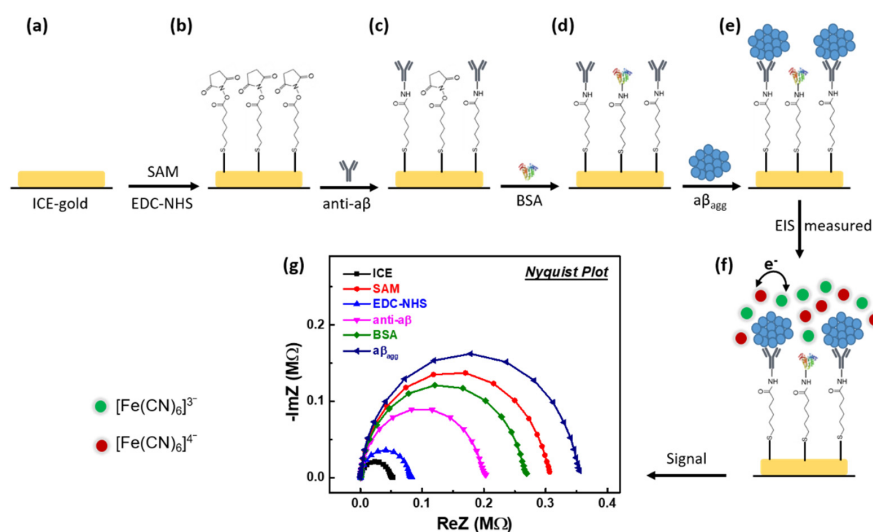
Figure 2. (**a–e**) Development procedure the immunosensor anti-aβ/SAM/ICE for the recognition aβ$_{agg}$, (**f**) impedimetric measurement mechanism in the recognition aβ$_{agg}$ by the developed biosensor anti-aβ/SAM/ICE, and (**g**) impedimetric results represent by Nyquist plot at each step of the development anti-aβ/SAM/ICE biosensor in the recognition aβ$_{agg}$.

2.3. EIS Measurements and Functional Group Characterization

EIS was performed using EC-Lab (SP-200, Bio-Logic, France) in 5 mM [Fe(CN)$_6$]$^{3-/4-}$ in PBS (pH 7.4) at each step of the anti-aβ/SAM/ICE biosensor development and various time intervals of the disaggregation process of aβ$_{agg}$. The EIS data was obtained by putting on a 10 mV of sinus amplitude which satisfy the linear properties of electrical response of the object between the working and reference electrode from 100 mHz to 1 MHz of range frequency. Z-Fit software (EC-Lab, Bio-Logic, France) was used to fit the obtained EIS data through by the Randle's equivalent circuit.

Fourier-transform infrared (FT-IR) spectra was characterized by using Jasco-4600 FTIR (USA) spectrometer to confirm the functional groups for the fabrication steps of the anti-aβ/SAM/ICE biosensor.

3. Results and Discussion

3.1. Investigating the Development of Impedimetric Immunosensor

As shown in Figure 3a, EIS measurements were carried out to determine the Nyquist-plots with the imaginary impedance component (-Im(Z)) plotted with the actual impedance component (Re(Z)) to confirm the successful modification of substantial ingredients to the electrode surface at different stages of the development the anti-aβ/SAM/ICE immunosensor.

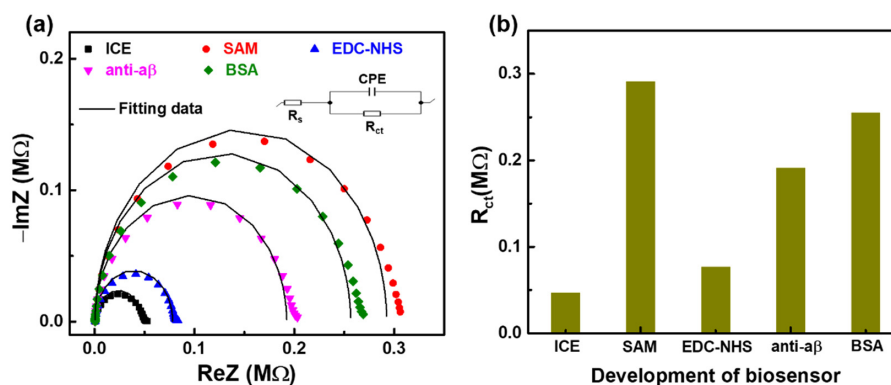**Figure 3.** EIS results at each step of the development of biosensor anti-aβ/SAM/ICE display in (**a**) Nyquist plots and (**b**) charge-transfer resistance (R$_{ct}$).

The equivalent circuit model of Randle insert into Figure 3a was used to fit the Nyquist plot data, showing three EIS parameters, including the C (capacitance for the electrode-solution interface element), R_{ct} (interfacial charge-transfer resistance that corresponds to the semicircular diameter in the Nyquist plot), and R_s (solution resistance).

The obtained fitting value of R_{ct} from Figure 3a was displayed in Figure 3b and Table 1. After SAM deposition that can be attributed to the $-COO^-$ group and the carbon chain SAM which prevents the transfer of the negative charged $[Fe(CN)_6]^{3-/4-}$ redox couple to the electrode surface, the value of R_{ct} has increased dramatically. Then, R_{ct} decreased after the EDC–NHS layer was deposited on the SAM-modified electrode, suggesting that the $-COO^-$ groups of SAM were activated with the EDC–NHS carbodiimide coupler, the formation of succinimide ester on the modified electrode surface of SAM allows fast electron transfer between the electrode and the interface [19]. The two continuous immobilization steps of anti-aβ and BSA showed an increase in R_{ct} due to the binding of a specific material on the sensor surface which enhanced its surface resistance [20], demonstrating that the surface of the biosensor was covered by specific materials.

Table 1. EIS parameters of the bare and modified ICE extrapolated by fitting the measured spectra to the equivalent circuit model shown in Figure 3a.

Electrode	R_s (Ω)	C (F)	R_{ct} (Ω)
ICE	529.3	55.37×10^{-9}	47,294
SAM	522.8	77.78×10^{-9}	291,956
EDC-NHS	524.9	69.69×10^{-9}	77,691
anti-aβ	524	75.88×10^{-9}	191,820
BSA	504.5	76.49×10^{-9}	255,926

Fourier-transform infrared (FT-IR) spectra was also used to confirm the fabrication of the anti-aβ/SAM/ICE biosensor, and the results were displayed in Figure 4. The FT-IR result of the SAM-modified ICE showed the typical peaks near 1601 cm^{-1} of carbonyl from the carboxylic acid moiety on the alkanethiols of SAM [21], indicating the immobilization of SAM on the ICE. FT-IR result of the immobilized anti-aβ on the EDC-NHS coupler activated SAM-modified ICE (blue curve in Figure 4) showed the typical peaks of protein at near 3374 cm^{-1} of N-H stretching of amide II [22], 2925 and 2849 cm^{-1} of C-H stretching of -CH$_2$ of protein [23,24], 920 cm^{-1} of C-O stretching [25], and 602 cm^{-1} of N-H deformation [22], which demonstrated the successful development of the anti-aβ/SAM/ICE biosensor.

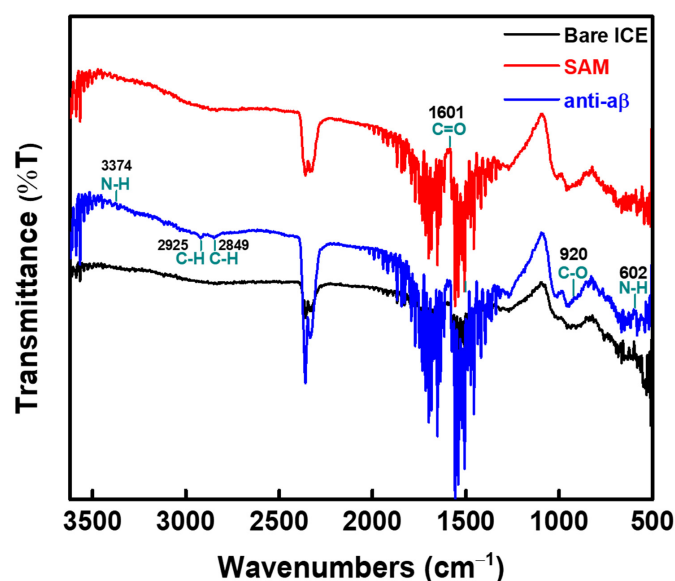**Figure 4.** FT-IR results for the fabrication of the anti-aβ/SAM/ICE biosensor.

3.2. Monitoring the Effect of EPPS on aβ Disaggregation

EPPS was used to target the disaggregation of aβ$_{agg}$ into its monomeric form. To confirm whether EPPS had an effect on the disaggregation of aβ$_{agg}$, EIS was used to explore the change in R$_{ct}$ of the specific anti-aβ/SAM/ICE biosensor for recognizing aβ during incubation with EPPS at different time intervals.

Firstly, the impact of EPPS on the anti-aβ antibody was studied. EIS measurements of the anti-aβ/SAM/ICE biosensor after incubation with 20 mM·L^{-1} EPPS at different time intervals are displayed in Figure 5. The Nyquist plots in Figure 5a did not change significantly after treatment with EPPS. Using Randle's equivalent circuit to fit the EIS data of Nyquist plots in Figure 5a, the R$_{ct}$ value was generated that serve to normalize the response of the anti-aβ/SAM/ICE biosensor to the EPPS treatment at 10, 20, 30, 40, 50 min in Figure 5b, where R$_0$ represents the R$_{ct}$ value of the biosensor with the immobilization of anti-aβ antibody, and R$_a$ represents the R$_{ct}$ value of the anti-aβ/SAM/ICE biosensor within the treatment of EPPS. The normalized value $(R_a - R_0)/R_0$ of the anti-aβ/SAM/ICE biosensor in Figure 5b did not change significantly after treatment with EPPS at various time periods, indicating that EPPS did not affect the anti-aβ antibody. The fitting EIS data were shown in Table 2.
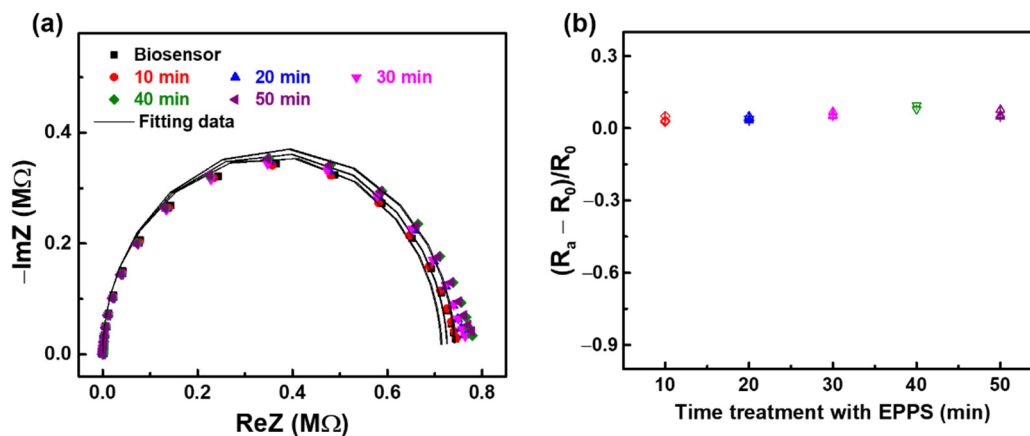

Figure 5. EIS results of the biosensor anti-aβ/SAM/ICE with the treatment in EPPS at different time intervals display in (**a**) Nyquist plots and (**b**) Normalization of R$_{ct}$. (*n* = 3; three data points shown).

Table 2. EIS parameters of the anti-aβ/SAM/ICE biosensor after treatment with EPPS at different time intervals, extrapolated by fitting the measured spectra in Figure 5a to the equivalent circuit model of Randle.

Electrode	R$_s$ (Ω)	C (F)	R$_{ct}$ (Ω)
Biosensor	490.9	55.55×10^{-9}	715,084
10 min	491.9	56.72×10^{-9}	724,551
20 min	487.5	57.66×10^{-9}	726,538
30 min	488.7	57.93×10^{-9}	724,904
40 min	488.5	58.36×10^{-9}	743,262
50 min	486.3	58.83×10^{-9}	730,896

Gel electrophoresis method [26] was used to confirm the aggregation state of aβ in this manuscript. As seen in Figure 6, the gel electrophoresis result of aβ$_{agg}$ showed the molecular-weight ranging of 11 kDa for oligomer form, which corresponds to a smear band containing monomers and low-molecular-weight oligomers ranging between 4 and 18 kDa in size of aβ oligomers [27], demonstrating the oligomeric form of aβ$_{agg}$ in this research.
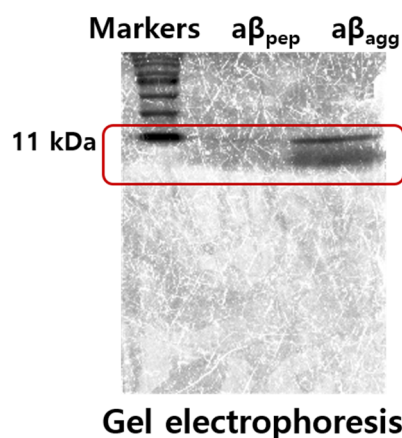
Figure 6. Gel electrophoresis results of $a\beta_{pep}$ and $a\beta_{agg}$.

The process of disaggregation of $a\beta_{agg}$ by EPPS at different time intervals is described in Section 2.2. Initially, the anti-$a\beta$/SAM/ICE biosensor was incubated with $a\beta_{agg}$ (2.5×10^{-3} mg·mL^{-1}) for 20 min in the absence of EPPS and measured via EIS to examine the $a\beta$ recognition of the biosensor. EIS measurements showed an increase in the diameter and height of the semicircle in the Nyquist plot, corresponding to the enhanced R_{ct} after the anti-$a\beta$/SAM/ICE biosensor was incubated with $a\beta_{agg}$, which is marked by 0 min in Figure 7a. This enhancement of R_{ct} is ascribed to the hindrance of electron transfer between the $[Fe(CN)_6]^{3-/4-}$ redox couple and the electrode surface due to successful specific binding between anti-$a\beta$ antibody and $a\beta_{agg}$, called $a\beta_{agg}$ complex on the surface of the sensor. The biosensor with the $a\beta_{agg}$ complex was subsequently incubated for different time periods (10, 20, 30, 40, and 50 min) with 20 mM·L^{-1} of EPPS and was used for EIS measurements. As shown in Figure 7a, after 10 min of incubation in EPPS, the R_{ct} of the biosensor with the $a\beta_{agg}$ complex in the Nyquist plot showed an increase in the height and diameter of the semicircle, and the Nyquist plot remained the same for the next 20 min of incubation with EPPS, which indicated that the $[Fe(CN)_6]^{3-/4-}$ ion transport towards the electrode surface was blocked due to excessive $a\beta$ on the electrode surface. These results implied that the disaggregation of $a\beta_{agg}$ started after 10 min of incubation with EPPS and was continuously maintained after 20 min of incubation. This disaggregation process converted the $a\beta_{agg}$ into small $a\beta$ monomers, and still retained a certain amount of $a\beta_{agg}$, creating an abundant compound of $a\beta$ monomers and $a\beta_{agg}$ on the biosensor surface, as delineated in Figure 8a, which hindered the transportation of $[Fe(CN)_6]^{3-/4-}$ redox couple to the electrode surface, leading to an increase in R_{ct}. Figure 7a showed the decline in R_{ct} after treatment with EPPS at 30 min, which manifested the disaggregation of the remaining $a\beta_{agg}$ into several monomeric $a\beta$ molecules on the sensor surface, suggesting that the movement of ion $[Fe(CN)_6]^{3-/4-}$ toward the electrode surface was facilitated; the impeded ion $[Fe(CN)_6]^{3-/4-}$ movement was caused by the presence of a dense $a\beta_{agg}$ that was reduced by converting the $a\beta_{agg}$ molecules into $a\beta$ monomers, leading to the expansion of spacing between the specific $a\beta$ molecules on the electrode surface, resulting in facilitating transport of redox couple $[Fe(CN)_6]^{3-/4-}$. This decline of R_{ct} continued to occur at 40 and 50 min during EPPS treatment, which indicated the continuous disaggregation of $a\beta_{agg}$. A graphical description of the disaggregation process of $a\beta_{agg}$ by EPPS at various time intervals is shown in Figure 8a. The response of $a\beta_{agg}$ to EPPS treatment at time periods was evaluated by normalizing the R_{ct} value of Figure 7a and plotted against time, as $(R_b - R_i)/R_i$ in Figure 7b, where R_i represents the R_{ct} of the biosensor with the immobilization of $a\beta_{agg}$, and R_b represents the R_{ct} of the biosensor with the immobilization of $a\beta_{agg}$ within the EPPS treatment. The normalized value $(R_b - R_i)/R_i$ in Figure 7b increased after 10 min of EPPS treatment, remained stable after 20 min, and gradually decreased over the 30, 40, and 50 min points, which indicated the disaggregation process of $a\beta_{agg}$ at different time intervals starting at 10 min and confirmed the effect of EPPS on $a\beta_{agg}$ disag-

gregation, corresponding to the results and explanation in Figure 7a. A detailed graphical description of the disaggregation process of aβ$_{agg}$ by EPPS at various time intervals is provided in Figure 8a. The fitting EIS data were shown in Table 3.
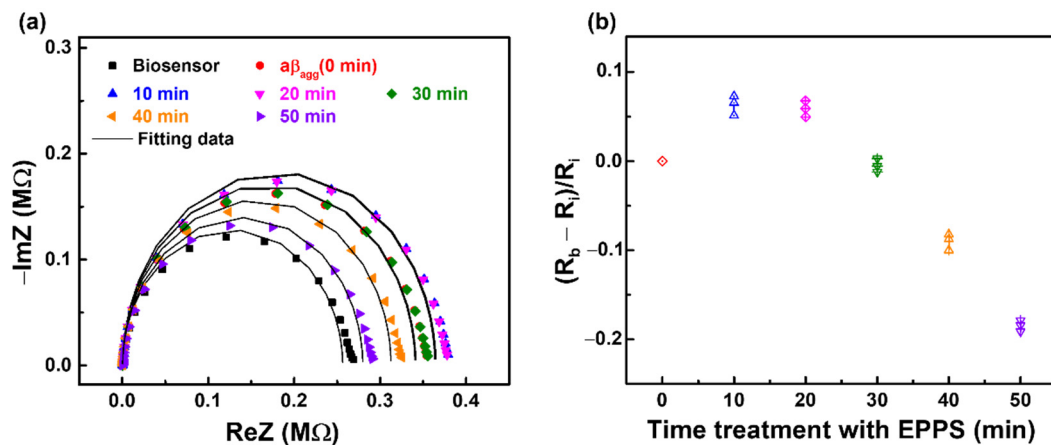

Figure 7. EIS results monitoring the disaggregation aβ$_{agg}$ with the treatment in EPPS at different time intervals display in (**a**) Nyquist plots and (**b**) Normalization of R$_{ct}$. (*n* = 3; three data points shown).
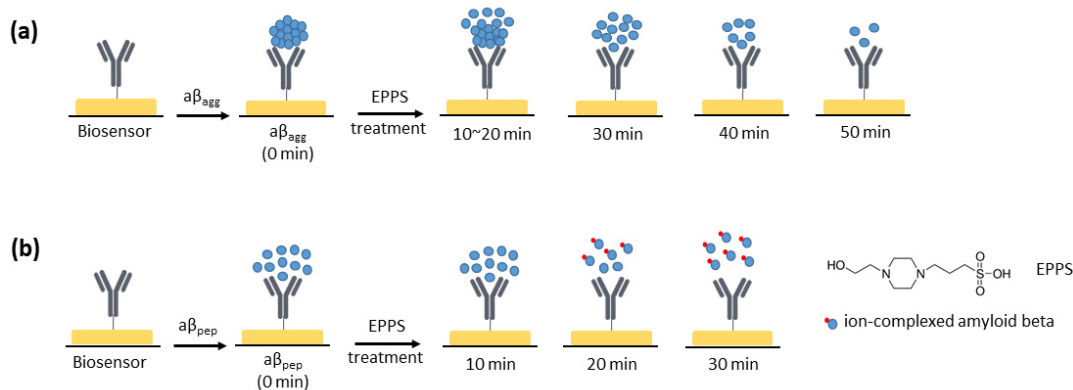

Figure 8. (**a**) Disaggregation mechanism of aβ$_{agg}$ by EPPS, and (**b**) the impact of EPPS on aβ$_{pep}$.

Table 3. EIS parameters of the anti-aβ/SAM/ICE biosensor after incubating with aβ$_{agg}$, and then conduct to treatment with EPPS at different time intervals, extrapolated by fitting the measured spectra in Figure 7a to the equivalent circuit model of Randle.

Electrode	R$_s$ (Ω)	C (F)	R$_{ct}$ (Ω)
Biosensor	504.8	76.10×10^{-9}	228,331
aβ$_{agg}$ (0 min)	519.2	76.29×10^{-9}	331,631
10 min	517.4	75.98×10^{-9}	366,841
20 min	517.1	75.89×10^{-9}	363,145
30 min	519.1	75.08×10^{-9}	334,918
40 min	519.5	74.81×10^{-9}	307,364
50 min	517.6	74.71×10^{-9}	274,678

The effect of EPPS on the aβ 1–42 peptide (aβ$_{pep}$), a long peptide of 1–42 amino acids, was also studied for comparison with the obtained results of aβ$_{agg}$, which are mentioned above. The experiment of aβ$_{pep}$ treatment in EPPS was carried out through similar processes as described in Section 2 with aβ$_{agg}$ replaced by aβ$_{pep}$. Nyquist plot of EIS result in Figure 9a show an increase in R$_{ct}$ of the biosensor anti-aβ/SAM/ICE after 20 min of incubation with aβ$_{pep}$. This increment of R$_{ct}$ is expected due to the repulsion

between the negative charge of immobilized $a\beta_{pep}$ antigen on the anti-$a\beta$/SAM/ICE biosensor with redox couple, that could prevent the redox couple from reaching the SAM-modified electrode, confirming the successful binding between anti-$a\beta$ and $a\beta_{pep}$ [28]. The R_{ct} of the biosensor with the immobilized $a\beta_{pep}$ remained the same after 10 min of treatment in EPPS, indicating that $a\beta_{pep}$ was not affected by EPPS for the initial 10 min treatment. R_{ct} significantly decreased after 20 and 30 min of subsequent EPPS treatment, indicating the facilitating electron transfer at the electrode interface. This decrease of R_{ct} may be attributed to the fragmentation of $a\beta_{pep}$ by EPPS, leading to the formation of ion-complexed amyloid beta with $[Fe(CN)_6]^{3-/4-}$ [29,30], which results in the decreasing of R_{ct} and enhancing of electrochemical property of the sensor at 20 min treatment, and at more treatment time of 30 min [16]. The normalized result $(R_b - R_i)/R_i$ is displayed in Figure 9b, where R_i represents the R_{ct} of the biosensor with the immobilization of $a\beta_{pep}$, and R_b represents the R_{ct} of the biosensor with the immobilization of $a\beta_{pep}$ within the EPPS treatment, which corresponds with the data of Nyquist plots in Figure 9a. The $(R_b - R_i)/R_i$ was stable after 10 min, and rapidly decreased over the 20 and 30 min points following EPPS treatment. Figure 8b shows the effect of EPPS treatment on $a\beta_{pep}$, and EIS results are shown in Figure 9. The fitting EIS data were shown in Table 4.
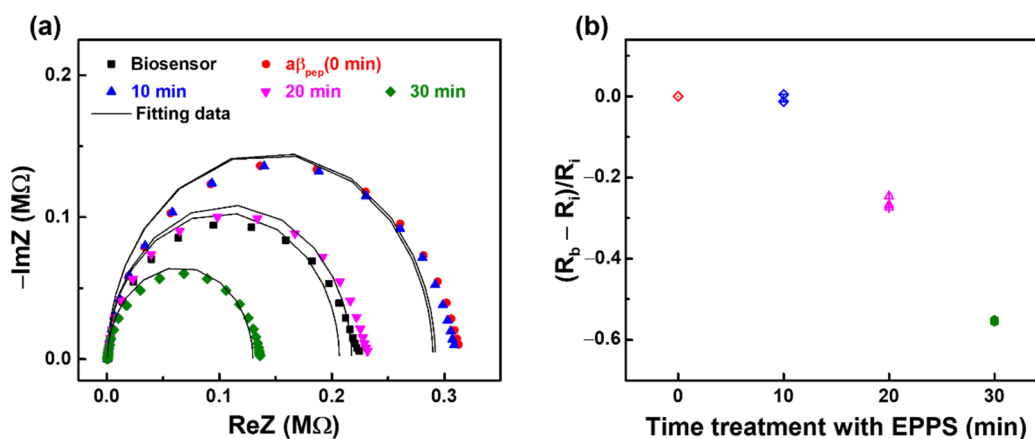

Figure 9. EIS results monitoring the impact of EPPS on the $a\beta_{pep}$ at different time intervals display in (**a**) Nyquist plots and (**b**) Normalization of R_{ct}. (*n* = 3; three data points shown).

Table 4. EIS parameters of the anti-$a\beta$/SAM/ICE biosensor after incubating with $a\beta_{pep}$, and then conduct to treatment with EPPS at different time intervals, extrapolated by fitting the measured spectra in Figure 9a to the equivalent circuit model of Randle.

Electrode	R_s (Ω)	C (F)	R_{ct} (Ω)
Biosensor	633.5	91.3×10^{-9}	205,978
$a\beta_{pep}$ (0 min)	635	92.96×10^{-9}	289,018
10 min	632.6	92.17×10^{-9}	289,110
20 min	629.8	90.69×10^{-9}	209,893
30 min	639.9	88.06×10^{-9}	129,281

By examining the EIS results of $a\beta_{agg}$ and $a\beta_{pep}$ in the treatment with EPPS in this study, it is observed that EPPS affects the disaggregation of $a\beta_{agg}$ gradually and leads to the establishment of a disaggregation mechanism, as shown in Figure 8, while EPPS causes rapid disruption of $a\beta_{pep}$.

3.3. Kinetic Disaggregation Rate k

The kinetic disaggregation rate *k* of protein is an important parameter in evaluating the functioning of neurodegenerative diseases [31]. However, there have not been report

on the k value for $a\beta_{agg}$ at present. To estimate the disaggregation rate k value for $a\beta_{agg}$, the normalized data for the treatments of $a\beta_{agg}$ and $a\beta_{pep}$ in EPPS were plotted and fitted versus time, as shown in Figure 10. Data for the disaggregation experiment $a\beta_{agg}$ represent the best fit of the data to a single-exponential function y = *0.149 − 0.048*exp(*0.038*x), whereas data for the treatment $a\beta_{pep}$ in EPPS express a linear fit function y = *0.271 − 0.027*x. According to the studies of kinetic disaggregation of proteins, the fitting data for protein disaggregation has been expressed by an exponential function F = y_0 + Aexp($-k$t) [31,32], where k represents the disaggregation rate. Consequently, the disaggregation rate k of $a\beta_{agg}$ was determined to be 0.038 by our method, providing a reference parameter for the disaggregation of $a\beta_{agg}$ for future studies.
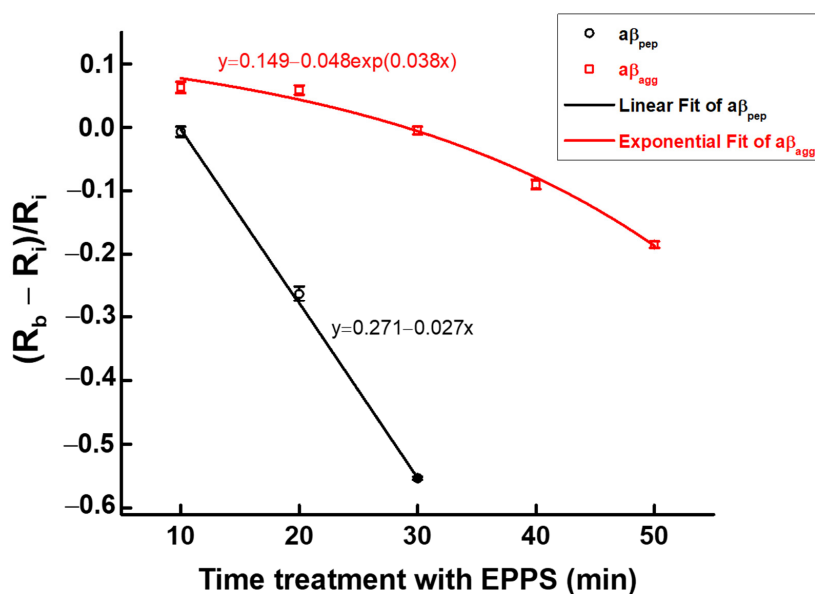

Figure 10. Fitting of two sets of disaggregation data for $a\beta_{agg}$ and $a\beta_{pep}$, respectively; symbols and bars represent the average and standard deviation of the data (n = 3).

4. Conclusions

A new concept of measuring $a\beta_{agg}$ disaggregation following treatment with EPPS via EIS signaling was introduced in this report. An electrochemical impedimetric immunosensor was developed to monitor EIS signals at the disaggregation stages of $a\beta_{agg}$ during treatment with EPPS at different time intervals. The obtained EIS results confirmed that the disaggregation of $a\beta_{agg}$ by treatment in EPPS occurred after 10 min, and this disaggregation process continued gradually over the next 50 min. A single exponential function for $a\beta_{agg}$ disaggregation was also found in this report, with a kinetic disaggregation rate (k) value of 0.038. The data indicated the successful application of EIS measurement in monitoring and establishing the mechanism for the impact of EPPS on the disaggregation of $a\beta_{agg}$, which may lead to new insights in the diagnosis and treatment of signs of AD at various phases.

Informed Consent Statement: Not applicable.

Data Availability Statement: Not applicable.

Conflicts of Interest: The authors declare no conflict of interest.

References

1. Murphy, M.P.; LeVine, H., III. Alzheimer's Disease and the β-Amyloid Peptide. *J. Alzheimer's Dis.* **2010**, *19*, 311. [CrossRef] [PubMed]
2. Blennow, K.; Mattsson, N.; Schöll, M.; Hansson, O.; Zetterberg, H. Amyloid biomarkers in Alzheimer's disease. *Trends Pharmacol. Sci.* **2015**, *36*, 297–309. [CrossRef] [PubMed]
3. Clifford, R.J., Jr.; Bennett, D.A.; Blennow, K.; Carrillod, M.C.; Dunne, B.; Haeberleinf, S.B.; Holtzmang, D.M.; Jagusth, W.; Jesseni, F.; Karlawishj, J.; et al. NIA-AA Research Framework: Toward a biological definition of Alzheimer's disease. *Alzheimer's Dement.* **2018**, *14*, 535–562.
4. O'Brien, R.J.; Wong, P.C. Amyloid Precursor Protein Processing and Alzheimer's Disease. *Annu. Rev. Neurosci.* **2011**, *34*, 185–204. [CrossRef] [PubMed]
5. Yagi, H.; Ozawa, D.; Sakurai, K.; Kawakami, T.; Kuyama, H.; Nishimura, O.; Shimanouchi, T.; Kuboi, R.; Naiki, H.; Goto, Y. Laser-induced Propagation and Destruction of Amyloid β Fibrils. *J. Biol. Chem.* **2010**, *285*, 19660–19667. [CrossRef] [PubMed]
6. Lee, W.S.; Jung, H.H.; Son, M.G.; Lee, H.B.; Kwak, T.J.; Lee, G.D.; Kim, C.H.S.; Lee, W.; Yoon, D.S. Characterization of the regrowth behavior of amyloid-like fragmented fibrils decomposed by ultrasonic treatment. *RSC Adv.* **2014**, *4*, 56561–56566. [CrossRef]
7. Takeda, T.; Klimov, D.K. Temperature-Induced Dissociation of Aβ Monomers from Amyloid Fibril. *Biophys. J.* **2008**, *95*, 1758–1772. [CrossRef]
8. Bayliss, D.L.; Walsh, J.L.; Shama, G.; Iza, F.; Kong, M.G. Reduction and degradation of amyloid aggregates by a pulsed radio-frequency cold atmospheric plasma jet. *New J. Phys.* **2009**, *11*, 115024. [CrossRef]
9. Sacchettini, J.C.; Kelly, J.W. Therapeutic strategies for human amyloid diseases. *Nat. Rev. Drug Discov.* **2002**, *1*, 267–275. [CrossRef]
10. Karran, E.; Mercken, M.; Strooper, B.D. The amyloid cascade hypothesis for Alzheimer's disease: An appraisalfor the development of therapeutics. *Nat. Rev. Drug Discov.* **2011**, *10*, 698–712. [CrossRef]
11. Gerlinde, G.; Albrecht, O.; Mario, L.; Ronald, F.F.; Erich, E.W.; Jan, B. Black tea theaflavins inhibit formation of toxic amyloid-β and α-synuclein fibrils. *Biochemistry* **2011**, *50*, 10624–10636.
12. Lee, J.W.; Lee, Y.K.; Ban, J.O.; Ha, T.Y.; Yun, Y.P.; Han, S.B.; Oh, K.W.; Hong, J.T. Green tea (-)-epigallocatechin-3-gallate inhibits beta-amyloid-induced cognitive dysfunction through modification of secretase activity via inhibition of ERK and NF-kappaB pathways in mice. *J. Nutr.* **2009**, *139*, 1987–1993. [CrossRef] [PubMed]
13. Cheng, B.; Liu, X.; Gong, H.; Huang, L.; Chen, H.; Zhang, X.; Li, C.; Yang, M.; Ma, B.; Jiao, L.; et al. Coffee Components Inhibit Amyloid Formation of Human Islet Amyloid Polypeptide in Vitro: Possible Link between Coffee Consumption and Diabetes Mellitus. *J. Agric. Food Chem.* **2011**, *59*, 13147–13155. [CrossRef] [PubMed]
14. Kim, H.Y.; Kim, H.V.; Jo, S.M.; Lee, C.J.; Choi, S.Y.; Kim, D.J.; Kim, Y.S. EPPS rescues hippocampus-dependent cognitive deficits in APP/PS1 mice by disaggregation of amyloid-β oligomers and plaques. *Nat. Commun.* **2015**, *6*, 8997. [CrossRef] [PubMed]
15. Yoo, Y.K.; Kim, J.S.; Kim, G.; Kim, Y.S.; Kim, H.Y.; Lee, S.J.; Cho, W.W.; Kim, S.S.; Lee, S.M.; Lee, B.C.; et al. A highly sensitive plasma-based amyloid-β detection system through medium-changing and noise cancellation system for early diagnosis of the Alzheimer's disease. *Sci. Rep.* **2017**, *7*, 8882. [CrossRef]
16. Rushworth, J.V.; Ahmed, A.; Griffiths, H.H.; Pollock, N.M.; Hooper, N.M.; Millner, P.A. A label-free electrical impedimetric biosensor for the specific detection of Alzheimer's amyloid-beta oligomers. *Biosens. Bioelectron.* **2014**, *56*, 83–90. [CrossRef]
17. Xing, Y.; Feng, X.Z.; Zhang, L.; Hou, J.; Han, G.C.; Chen, Z. A sensitive and selective electrochemical biosensor for the determination of beta-amyloid oligomer by inhibiting the peptide-triggered in situ assembly of silver nanoparticles. *Int. J. Nanomed.* **2017**, *12*, 3171–3179. [CrossRef]
18. Truong, T.N.L.; Takamura, Y.; Tamiya, E.; Vestergaard, M.C. Modified screen printed electrode for development of a highly sensitive label-free impedimetric immunosensor to detect amyloid beta peptides. *Anal. Chim. Acta* **2015**, *892*, 69–76.
19. Chinnadayyala, S.R.; Cho, S.B. Electrochemical Immunosensor for the Early Detection of Rheumatoid Arthritis Biomarker: Anti-Cyclic Citrullinated Peptide Antibody in Human Serum Based on Avidin-Biotin System. *Sensors* **2021**, *21*, 124. [CrossRef]
20. Martic, S.; Rains, M.K.; Kraatz, H.B. Probing copper/tau protein interactions electrochemically. *Anal. Biochem.* **2013**, *442*, 130–137. [CrossRef]
21. Smith, B.C. *Infrared Spectral Interpretation: A Systematic Approach*; CRC Press Inc.: Boca Raton, FL, USA, 1998.
22. Phan, L.M.T.; Kim, E.B.; Cheon, S.A.; Shim, T.S.; Kim, H.J.; Park, T.J. Reliable naked-eye detection of Mycobacterium tuberculosis antigen 85B using gold and copper nanoshell-enhanced immunoblotting techniques. *Sens. Actuators B Chem.* **2020**, *317*, 1282202. [CrossRef]
23. Gaddam, S.A.; Kotakadi, V.S.; Gopal, D.V.R.S.; Rao, Y.S.; Reddy, A.V. Efficent and robust biofabrication of silver nanoparticles by Cassia alata leaf extract and their antimicrobial activity. *J. Nanostruct. Chem.* **2014**, *4*, 82. [CrossRef]
24. Phan, L.M.T.; Rafique, R.; Baek, S.H.; Nguyen, T.P.; Park, K.Y.; Kim, E.B.; Kim, J.G.; Park, J.P.; Kailasa, S.K.; Kim, H.J.; et al. Gold-copper nanoshell dot-blot immunoassay for naked-eye sensitive detection of tuberculosis specific CFP-10 antigen. *Biosens. Bioelectron.* **2018**, *121*, 111–117. [CrossRef] [PubMed]

25. Kumar, M.H.V.; Gupta, Y.K. Effect of different extracts of Centella asiatica on cognition and markers of oxidative stress in rats. *J. Ethnopharmacol.* **2002**, *79*, 253–260. [CrossRef]
26. Smith, B.J. SDS Polyacrylamide Gel Electrophoresis of Proteins. *Proteins Methods Mol. Biol.* **1984**, *1*, 41–56. [PubMed]
27. An, S.S.A.; Lee, B.S.; Yu, J.S.; Lim, K.T.; Kim, G.J.; Lee, R.; Kim, S.W.; Kang, S.M.; Park, Y.H.; Wang, M.J.; et al. Dynamic changes of oligomeric amyloid β levels in plasma induced by spiked synthetic Aβ$_{42}$. *Alzheimer's Res. Ther.* **2017**, *9*, 86. [CrossRef]
28. Le, H.T.N.; Park, J.S.; Chinnadayyala, S.R.; Cho, S.B. Sensitive electrochemical detection of amyloid beta peptide in human serum using an interdigitated chain-shaped electrode. *Biosens. Bioelectron.* **2019**, *144*, 111694.
29. Lermyte, F.; Everett, J.; Yuko, P.Y.L.; Wootton, C.A.; Brooks, J.; Barrow, M.P.; Telling, N.D.; Sadler, P.J.; O'Connor, P.B.; Collingwood, J.F. Metal Ion Binding to the Amyloid β Monomer Studied by Native Top-Down FTICR Mass Spectrometry. *J. Am. Soc. Mass Spectrom.* **2019**, *30*, 2123–2134. [CrossRef]
30. Nair, G.N.; Perry, G.; Smith, M.A.; Reddy, V.P. NMR Studies of Zinc, Copper, and Iron Binding to Histidine, the Principal Metal Ion Complexing Site of Amyloid-β Peptide. *J. Alzheimer's Dis.* **2010**, *20*, 57–66. [CrossRef]
31. Cellmer, T.; Douma, R.; Huebner, A.; Prausnitz, J.; Blanch, H. Kinetic studies of protein L aggregation and disaggregation. *Biophys. Chem.* **2007**, *125*, 350–359. [CrossRef]
32. Priezzhev, A.V.; Ryaboshapka, O.M.; Firsov, N.N.; Sirko, I.V. Aggregation and Disaggregation of Erythrocytes in Whole Blood: Study by Backscattering Technique. *J. Biomed. Opt.* **1999**, *4*, 76–84. [CrossRef] [PubMed]